Heliyon 10 (2024) e34824

Contents lists available at ScienceDirect

Heliyon

journal homepage: www.cell.com/heliyon

Research article

Pressure-induced structural, electronic, optical, and mechanical properties of lead-free $GaGeX_3$ (X = Cl, Br and, I) perovskites: First-principles calculation

Md. Mehedi Hasan [a], Md. Amran Sarker [a], Mohshina Binte Mansur [a], Md. Rasidul Islam [b,*], Sohail Ahmad [c]

[a] Department of Materials Science & Engineering, Khulna University of Engineering & Technology (KUET), Khulna 9203, Bangladesh
[b] Department of Electrical and Electronic Engineering, Bangamata Sheikh Fojilatunnesa Mujib Science & Technology University, Jamalpur 2012, Bangladesh
[c] Department of Physics, College of Science, King Khalid University, P O Box 9004, Abha, Saudi Arabia

ARTICLE INFO

Keywords:
DFT
Renewable energy
Solar cell
Band gap
Density of states
Optoelectronics
Elastic stability

ABSTRACT

Researchers are now focusing on inorganic halide-based cubic metal perovskites that are not toxic as they strive to commercialize optoelectronic products and solar cells derived from perovskites. This study explores the properties of new lead-free compounds, specifically $GaGeX_3$ (where X = Cl, Br, and I), by executing first-principles Density Functional Theory (DFT) to analyze their optical, electronic, mechanical, and structural characteristics under pressure. Assessing the reliability of all compounds is done meticulously by applying the criteria of Born stability and calculating the formation energy. As discovered through elastic investigations, these materials showed anisotropic behavior, flexibility, and excellent elastic stability. The electronic band structures, calculated using both HSE06 and GGA-PBE functionals at 0 GPa, reveal fascinating behavior. However, computed band structures with non-zero pressures using GGA-PBE. Here, the conduction band moved to the lower energy when the halide Cl was changed with Br or I. In addition, the application of hydrostatic pressure can lead to tunable band gap properties in all compounds such as from 0.779 eV to 0 eV for $GaGeCl_3$, from 0.462 eV to 0 eV for $GaGeBr_3$ and from 0.330 eV to 0 eV for $GaGeI_3$, resulting transformation from semiconductor to metallic. Understanding the origins of bandgap changes can be illuminated by examining the partial and total density of states (PDOS & TDOS). When subjected to pressure, all the studied compounds showed an impactful increase in absorption coefficients and displayed exceptional optical conductivity in both the visible and UV zones. Yet, $GaGeCl_3$ is a more effective UV absorber because it absorbs light more strongly in the UV area. Moreover, $GaGeI_3$ stands out among the compounds examined due to its impressive visible absorption and optical conductivity, which remain consistent under varying pressure conditions. Besides, $GaGeI_3$ exhibits higher reflectivity when subjected to pressure making them suitable for UV shielding applications. At last, these metal cubic halide perovskites without lead present promising opportunities for advancing optoelectronic technologies. With their tunable properties and favorable optical characteristics, these materials are highly sought after for their potential in solar cells, multi-junctional solar cells, and different optoelectronic functions.

* Corresponding author.
E-mail address: rasidul@bsfmstu.ac.bd (Md.R. Islam).

https://doi.org/10.1016/j.heliyon.2024.e34824
Received 22 June 2024; Accepted 17 July 2024
Available online 18 July 2024

1. Introduction

The world's population is continuing to expand, which is driving up energy consumption. Having access to affordable, reliable, and abundant energy sources is crucial for our modern industrial society. Regrettably, finite resources such as fossil fuels are limited in supply and eventually deplete, serving as the primary source for our energy requirements. In addition, the combustion of fossil fuels results in the emission of greenhouse gases, contributing significantly to the overall global energy production. This further worsens the effects of climate change. Investigating alternate renewable energy sources, like solar power, is essential for reducing greenhouse gas emissions and addressing the effects of climate change [1–6]. In the fields of science and industry, solar cells have achieved a lot of interest and attention [7–11]. A solar cell comprises an upper electron transportation layer, a lower hole transportation layer, and a center absorber layer. The absorber layer normally absorbs light and generates electron-hole pairs. That's why, this layer is crucial in the solar cells structure. So, the physical characteristics of this layer such as optical, electronic, structural, and mechanical play a significant role in solar cell's performance.

Inorganic metal halide cubic perovskites have a higher solar cell efficiency than Si-based technology. These perovskites are used in a wide range of applications such as light-emitting diodes (LEDs), solar cells, energy conversion, and different optoelectronic systems because of their unique properties including long diffusion lengths, high mobility of charge carriers, low carrier recombination rates, and adjustable band gaps [12–14]. Also, these perovskites are economical and feasible when compared with Si-based technology [15–18]. The formula ABX_3 defines these perovskite structures where A and B are different types of cations and X is an anion. So, studying the physical characteristics of perovskite-based materials both theoretically and practically increases the scope of solar cells and various optoelectronics uses. As of right now, solar cells based on perovskites (PSCs) have a 22.1 % power conversion efficiency (PCE) [19], which represents a considerable advancement in their growth path. Despite having the greatest PCE of 25.2 % at the moment, lead-based perovskite solar cells are less durable because of their vulnerability to UV radiation, moisture, temperature, and humidity. The PCE of lead-free tin halide perovskites containing ethyl ammonium iodide, on the other hand, is 13 % [20]. Early organic PSCs using metallic Pb^{2+} were created, such as $CH_3NH_3PbI_3$ (or $MAPbX_3$) [21,22], but they ran into toxicity issues, especially because lead (Pb) is known to be dangerous. As such, efforts have been focused on replacing Pb^{2+} with non-toxic cations like Ge^{2+} and Sn^{2+} or using substitute A^+ cations instead of their organic equivalents [23]. The continuous quest to produce lead-free halide-based perovskites is one of the main impediments to the commercial viability of perovskite-based solar cells.

To improve the performance of optoelectronic devices, pressure is an important factor. For regulating the physical and chemical characteristics of any kind of material, pressure plays a critical role [24,25]. Because pressure application may alter optical and electrical characteristics as well as induce structural changes, it is thought to be one of the practical ways to boost the solar energy conversion efficiency of these materials. Pressure-induced modifications can modify the band gap of the material, increase light absorption, decrease charge carrier recombination, and maximize charge separation [26–28]. For example, M. Aktary reported hydrostatic pressure effects of $CsPbX_3$ (X = Cl, Br, and I). Here, the electronic, optical responses were enhanced by applied pressure. Also, tuning the band gap of the compounds from semiconductor to metallic nature. In a recent study, we investigated the properties of cubic metal halide perovskites of $GaGeX_3$ (X = Cl, Br, and I) and examined their physical characteristics without the influence of pressure [29]. However, there is no comparative study on pressure-induced lead-free cubic halide $GaGeX_3$ (X = Cl, Br, and I) perovskites. This research investigates the potential of perovskite materials in solar energy conversion by examining how they respond to pressure-induced modification. Here, we incorporate Ge on the perovskite materials instead of Pb, and also, Ge-based perovskites exhibit enhanced optical absorption and conductivity [30,31]. We use Ga instead of CH_3NH_3 that's why remove the instability of organic compounds. Also, Ga has a low melting point, malleable nature, easily formable, non-toxic, corrosion-resistant, and semiconductor characteristics. That's why, in this research, we concentrate on Ga-based perovskites.

In this article, our objective is to obtain an understanding of the features of $GaGeX_3$ (X = Cl, Br, and I) under pressure and their potential as efficient lead-free photovoltaic materials by variation of pressure, systematically. This work examines the structural, electrical, mechanical, and optical properties of Ge-based halide $GaGeX_3$ (X = Cl, Br, and I) perovskites using first-principles simulations with applied pressure up to 15 GPa. Moreover, the study of the material's optical characteristics and structural stability is made easier by pressure, and these two aspects are essential for creating solar cells with increased efficiency. Therefore, our goal is to evaluate how perovskite structures' optoelectronic properties might be adjusted under various pressure levels to improve their applicability for multijunction solar cell applications.

2. Computational methodology

Using the CASTEP software [32], DFT-based calculations were conducted [33,34]. In order to determine the bandgap and electronic exchange-correlation energy, the GGA-PBE and HSE06 functionals were used [35]. It was thought that the presence of the ultrasoft pseudopotential of the Vanderbilt-type OTFG [36] would help control the electron interactions. The BFGS method was exercised to get the best possible crystal structure [37]. By adjusting the k-points to $7 \times 7 \times 7$ and the plane wave cutoff energy to 600 eV, the optimal structure and properties were computed. The Monkhorst-Pack method was applied to sample the k-points in the high-symmetry Brillouin zone, [38]. With larger k-points, optical properties were evaluated. The elastic constants of our models were estimated using the stress-strain method under normal conditions [39]. Using the CASTEP software, the elastic stiffness constants (C_{ij}) were determined, in accordance with the finite strain theory. Using the ELATE software, three-dimensional anisotropic contour plots for Young's modulus, Poisson's ratio, and Shear modulus parameters were represented. The optimal convergence factors were determined by ensuring that the total energy variation remained in the midst of 5×10^{-6} eV/atom, that the maximum

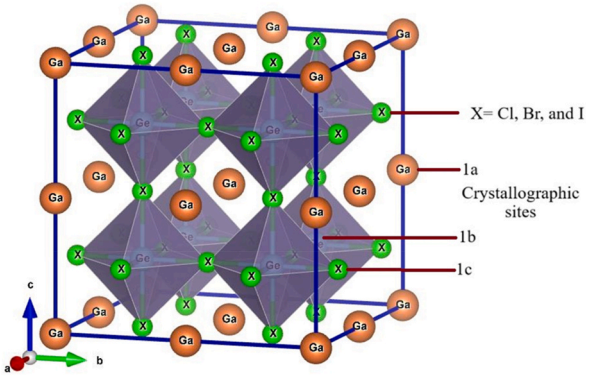

Fig. 1. This diagram illustrates the ABX_3 structure, accompanied by the supercell of $GaGeX_3$ (X = Cl, Br, and I) metal cubic halide perovskites.

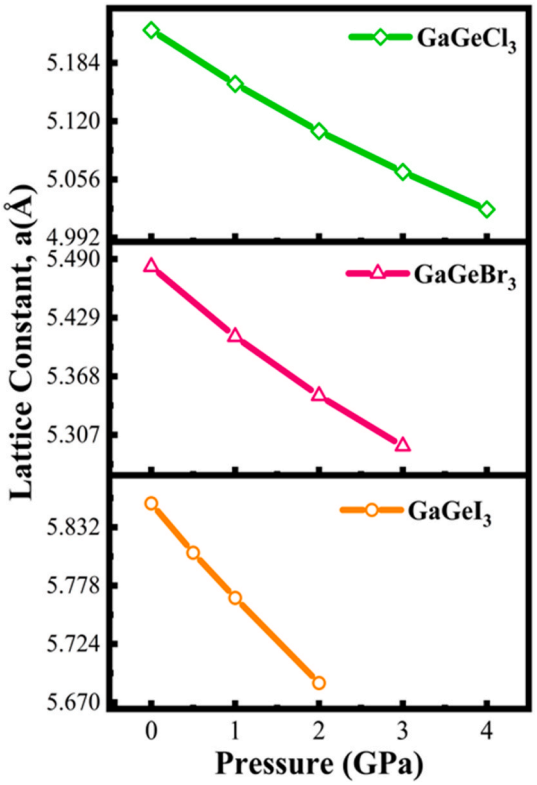

Fig. 2. Investigating the lattice constant of $GaGeX_3$ (X = Cl, Br, and I) compounds with the impact of pressures.

Hellmann-Feynman force was restricted to 0.01 eV/Å, that the maximum displacement was maintained at 5×10^{-4} Å, and that the maximum tension was maintained at 0.02 GPa. The optimal value for the strain magnitude was found that 0.003. The same convergence criteria were utilized that were mentioned before.

3. Results and discussions

3.1. Structural properties

Fig. 1 depicts the cubic crystal structure of $GaGeX_3$ (X = Cl, Br, and I) in a 3D schematic representation. Within this structure, Ga and Ge occupy specific Wyckoff coordinates: Ga is positioned at (0,0,0), while Ge is located at (0.5,0.5,0.5). Additionally, three X atoms are situated at (0.5,0,0.5), (0.5,0.5,0), and (0,0.5,0.5). This study focused on investigating three perovskites, which possess crystal structures of cubic and belong to space group 221: pm3m. Employing the GGA technique, various structural properties such as

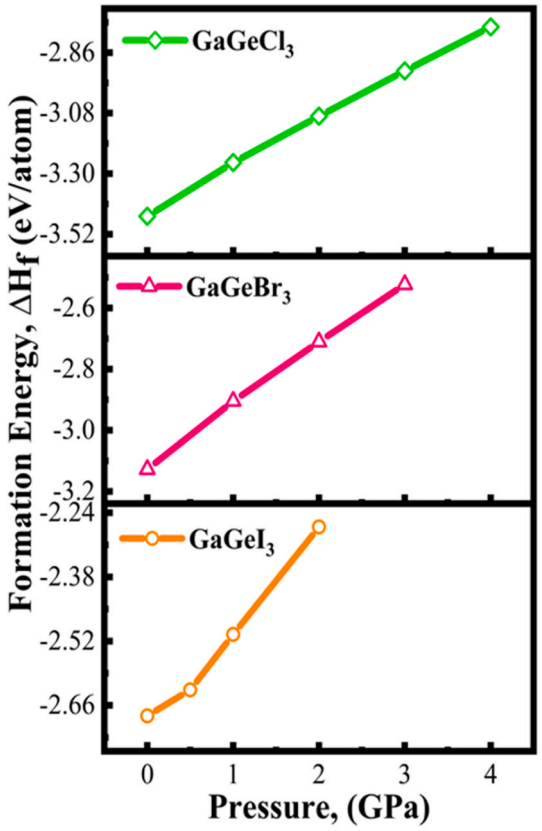

Fig. 3. Investigating the impact of pressure on $GaGeX_3$ (X = Cl, Br, and I) compounds' formation energy.

formation energy (ΔH_f), volume (V), and lattice constant (a) were determined through a volume optimization procedure to ascertain the stable ground state unit cell. Moreover, energy values relative to volume were matched to the Birch-Murnaghan equation of state [40]. Utilizing this fit, lattice parameters were computed under varying hydrostatic pressure conditions. The stability of $GaGeCl_3$, $GaGeBr_3$, and $GaGeI_3$ is contingent upon both the type and magnitude of applied stress. In this investigation, pressure was incrementally applied until these compounds transitioned into a metallic state. As positive pressure increases, the lattice parameter diminishes. Fig. 2 illustrates the variation in lattice parameters under applied compressive pressure. Supplementary Tables S1(a–c) presents a comprehensive record of lattice parameter values corresponding to different pressures. Analysis of Tables S1(a–c) indicates that as the halogen size escalates (from Cl to I), both the optimal lattice constant and volume expand.

Additionally, the thermodynamic and mechanical stability of $GaGeX_3$ are explored under varying pressures. The Born stability criteria are utilized to assess the stability of the mechanical of a compound derived from elastic constants.

$C_{11} + 2C_{12} > 0$, $C_{44} > 0$, $C_{11} - C_{12} > 0$

The estimated elastic constants of three materials fully meet this criterion, showing mechanical stability which will be further discussed in the mechanical section. The graph depicted in Fig. 3 illustrates the impact of pressure on the formation energy of $GaGeX_3$. The energies of $GaGeX_3$ are calculated using equation (1).

$$\Delta H_f(GaGeX_3) = \frac{[E_{tot.}(GaGeX_3) - E_s(Ga) - E_s(Ge) - 3E_s(X)]}{N} \quad (1)$$

Here, the total energy of the ground state of $GaGeX_3$ is represented by the symbol $E_{tot.}$ ($GaGeX_3$), while the energies of Ga, Ge, and X (where X can be Cl, Br, or I) per unit cell are represented by the symbols E_s (Ga), E_s (Ge), and E_s (X). The symbol N denotes the total atoms in a unit cell.

Based on the computed energy, it is evident that the energy (ΔH_f) exhibits negative values up to 4 GPa, 3 GPa, and 2 GPa for $GaGeCl_3$, $GaGeBr_3$, and $GaGeI_3$, respectively, under compressive stress, as indicated in Tables S1(a–c). Application of external compressive pressure results in further negativity in the formation energy of all compounds. The observed results with applied external pressure suggest that the $GaGeX_3$ structure being studied exhibits notable structural stability and tunability. Given perovskites' customizable structural and electrical characteristics, materials possessing desirable traits can be tailored for diverse applications. Supplementary Table S2 indicates that bond lengths decrease towards lower values in response to applied pressure, resulting from the unit

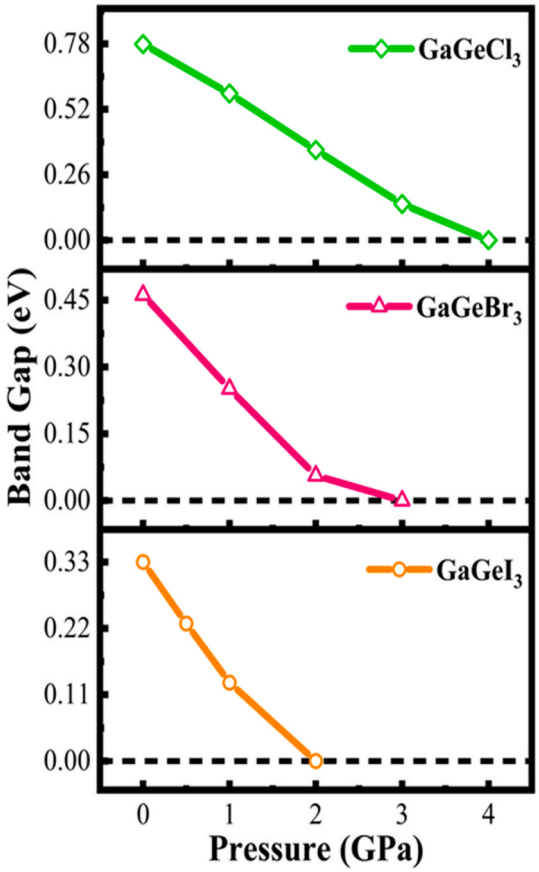

Fig. 4. Band gap value of $GaGeX_3$ (where X = Cl, Br, and I) changes based on the pressure.

cell's interatomic spaces contracting. When pressure is applied, the propensity of bond lengths to shorten indicates that the bonds between atoms are strengthened.

Moreover, it has been discovered that these compounds display direct band gaps and demonstrate semiconducting behavior. Consequently, they emerge as extremely favorable applicants for optoelectronic applications, notably in solar cells. The electrical and optical properties will be thoroughly discussed in the upcoming sections in order to provide additional validation for the results presented above.

3.2. Electronic properties

The electronic band structure (BS) and Density of States (DOS) are two methods used to gather information about the electronic properties of a material. We calculated the energy band structures (EBSs) of $GaGeX_3$ (X = Cl, Br, I) by analyzing the high symmetry route in k-space based on the energy regarding the Fermi energy ($E\text{-}E_F$). For the hydrostatic pressure (0–4 GPa), Figs. S1–3 illustrates the outcomes of band structure calculations, and the band gap changing by applied pressure is shown in Fig. 4. The shown EBSs have an energy spectrum that spans from −5 to 5 eV, encompassing the conduction band (CB) and the valence band (VB) located at the upper and lower ends of the structure, respectively. The Fermi position energy is denoted via the horizontal dashed red line, positioned at 0 eV. The predicted band gaps for the compounds of interest are shown in Tables S1(a–c) through tabular data. Fig. 5 displays the band gaps obtained through calculations using the HSE06 and PBE functional. Based on PBE, it can be observed that $GaGeCl_3$ has an energy gap of 0.779 eV at normal pressure. Its band nature is direct, specifically (R–R). However, when the Cl in $GaGeCl_3$ is substituted with larger halogens like Br and I, the band gap decreases to 0.462 eV for $GaGeBr_3$ and 0.330 eV for $GaGeI_3$. The HSE06 functional is employed to ascertain the precise band gap of the compounds. In the absence of pressure, the band gaps calculated using the HSE06 functional for $GaGeCl_3$, $GaGeBr_3$, and $GaGeI_3$ are in order, 1.632 eV, 1.284 eV, and 1.140 eV.

Based on PBE, the energy gap for $GaGeCl_3$ at zero pressure has been determined to be 0.770 eV, as illustrated in Fig. S1. As pressure increases, the R point conduction band minimum shifts closer to the Fermi energy level, suggesting the narrowing of the energy gap. At a pressure of 4 GPa, the VB maxima and the CB minima for $GaGeCl_3$ coincide. As a result, Eg disappears, which is evidence that $GaGeCl_3$ transforms from being semiconducting to being conducting [41]. The computed total and partial density of states (TDOS & PDOS) of all compounds are displayed in Figs. S4–6. Here the dashed line that is black located at 0 eV denotes the level of Fermi.

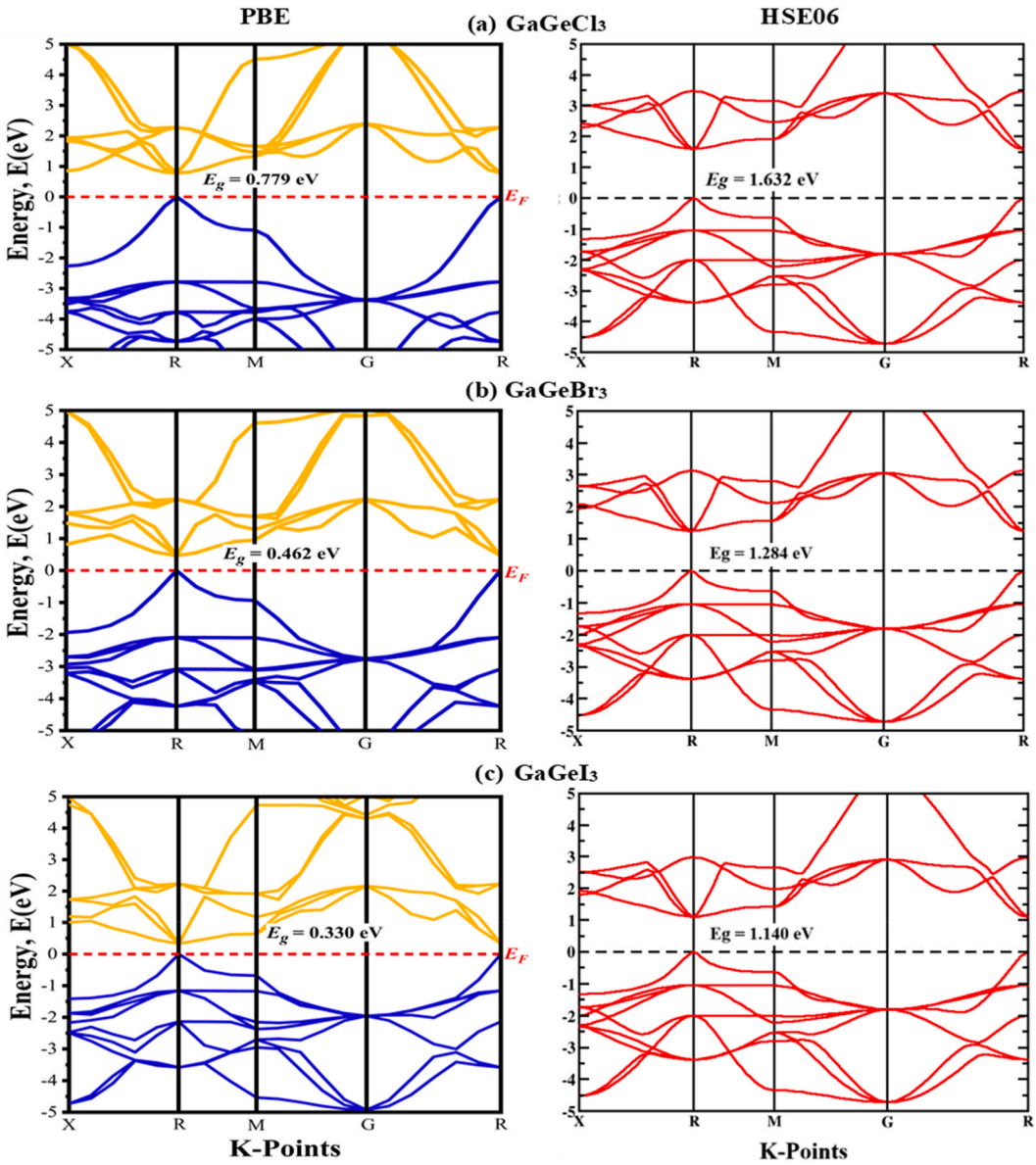

Fig. 5. Using the GGA-PBE and HSE06 functional, calculations of the electronic band structures of (a) $GaGeCl_3$, (b) $GaGeBr_3$, and (c) $GaGeI_3$.

Distinguishing the contribution to both the VBs and CBs is a frequent use of the DOS. $GaGeCl_3$ exhibits no TDOS value at E_F until 3 GPa, which further demonstrates its semiconducting nature. As the pressure for $GaGeCl_3$ rises to 4 GPa, the value of TDOS that is not zero indicates the shift from a semiconductor to a metal. Since all of the high points in the conduction band move steadily in the direction of the E_F as applied pressure increases, there is a significant pressure influence on TDOS. This leads to a shrinkage in the band gap energy, which is in alignment with the band structure shown in the Supplementary Fig. S1. The PDOS graph was employed to illustrate the elemental electronic contribution. The highest contribution was noted from the Cl-3p states, although the VBs of both under and without pressure of $GaGeCl_3$ systems also contained Ga-4s, Ga-4p, Ge-4s, and Ge-4p states. In contrast to the CBs, where Ga-4p states obviously predominate and all other states contribute just a little.

The electronic energy band structure of $GaGeBr_3$ was computed under pressure ranging from 0 to 3 GPa along the high symmetry regions, as seen in Fig. S2. Just like $GaGeCl_3$, at zero pressure, it has a band gap of 0.462 eV, making it a direct band semiconductor. It transitions to a metallic state ($E_g = 0$ eV) when the VB surpasses the Fermi level E_F and intersects with the CB at 3 GPa. To comprehend the electrical characteristics of $GaGeBr_3$ more clearly, the TDOS and the PDOS have been calculated and illustrated in Fig. S5. The zero TDOS value validates the semiconductors' band gap value found in Fig. S2. Increasing pressure leads to a drop in the TDOS value. In PDOS analysis, Br-4p makes up the majority of the atomic contribution seen in the VB, with a slight contribution of Ge-4p. Regarding

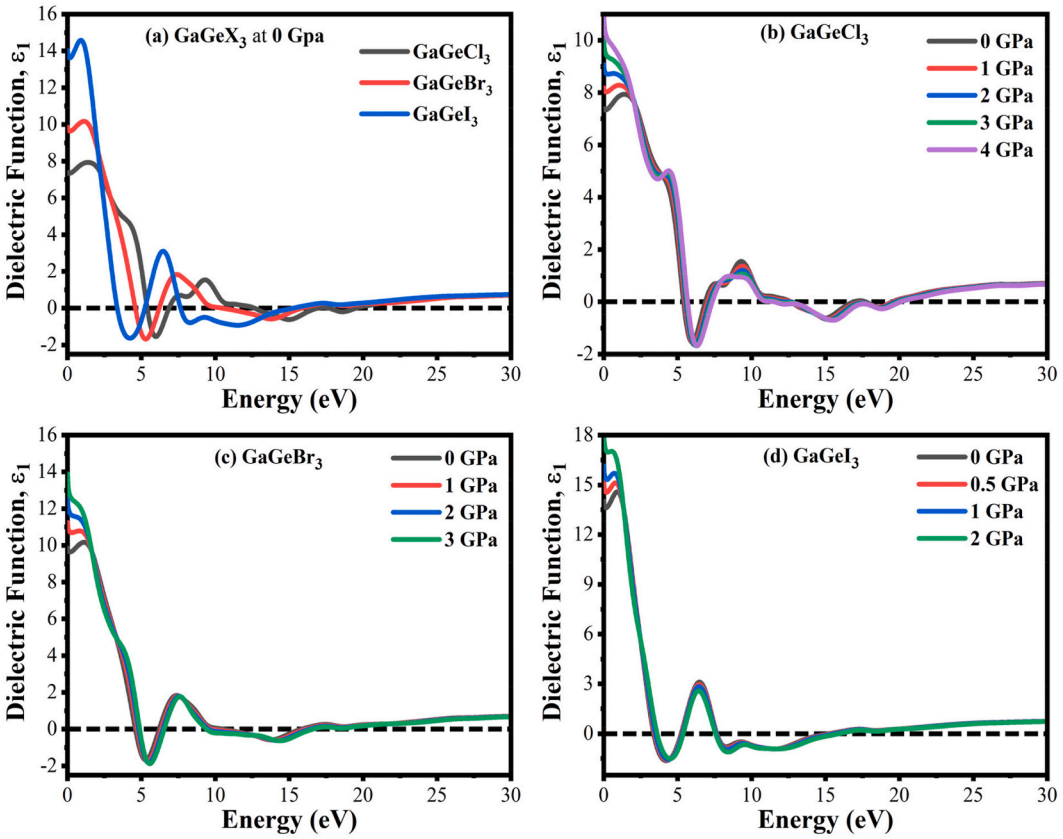

Fig. 6. Pressure-driven real component of $GaGeX_3$'s dielectric constant (where X = Cl, Br, and I).

the CB, the main contribution originates from Ga-4p, while Ge-4p and Cl-3p states make a minor contribution. As pressure increases, a peak shift towards the fermi level can be observed, suggesting a reduction in the band gap as shown in Fig. 4 [42].

An analogous electronic property is observed in $GaGeI_3$, with a band gap of 0.330 eV in its non-pressurized state. As Increasing in pressure that's why the semiconductor band shrinks, transitioning the material into a metallic state where the band gap is equal to zero at a pressure of 2 GPa. $GaGeI_3$ is also a direct narrow band gap semiconductor, just like $GaGeCl_3$ and $GaGeBr_3$, even if the transition into a metallic state occurs. The PDOS in Fig. S6 was used to demonstrate the electrical contribution of each constituent for $GaGeI_3$. The I-5p states made the most significant contribution, but the VBs of both under and without-pressure of $GaGeI_3$ systems also included Ga-4p, Ge-4s, and Ge-4p, I-5s states. Conversely, the CBs exhibit a preponderance of Ga-4p states and minimal contributions from the remaining states.

3.3. Optical properties

Scientific interest in metal halide perovskites has increased due to their remarkable optical characteristics, particularly within the fields of optoelectronics and photovoltaics. Additionally, it is essential to assess the optical properties in relation to applied pressure to advance material research toward the creation of optoelectronic devices and solar cell applications [43]. The characteristics of optical of $GaGeX_3$ (X = Cl, Br, I) under applied pressure which include the refractive index, dielectric's real and imaginary portion, conductivity, absorption, and reflectivity are discussed in this section using solar energy up to 30 eV. The most crucial optical property of a particular material is its dielectric function. Moreover, there is a significant correlation between the dielectric function and the electronic band structure because optical transitions that contribute to the dielectric function include electron migrations over various bands of energy. Examining additional optical properties requires first determining the dielectric function and it is $\varepsilon(\omega) = \varepsilon_1(\omega) + \varepsilon_2(\omega)$, where $\varepsilon_1(\omega)$, and $\varepsilon_2(\omega)$ represent the real and imaginary components of the dielectric function, respectively. The Kramer-Kronig connection [44] reveals the formula of the real part.

$$\varepsilon_1(\omega) = 1 + \frac{2}{\pi} P \int_0^{\infty} \frac{\omega' \varepsilon_2(\omega')}{\omega'^2 - \omega^2} d\omega'$$

The static dielectric function is clarified as the value of $\varepsilon_1(\omega)$ at 0 eV. It's a crucial indicator of how well optoelectronic devices

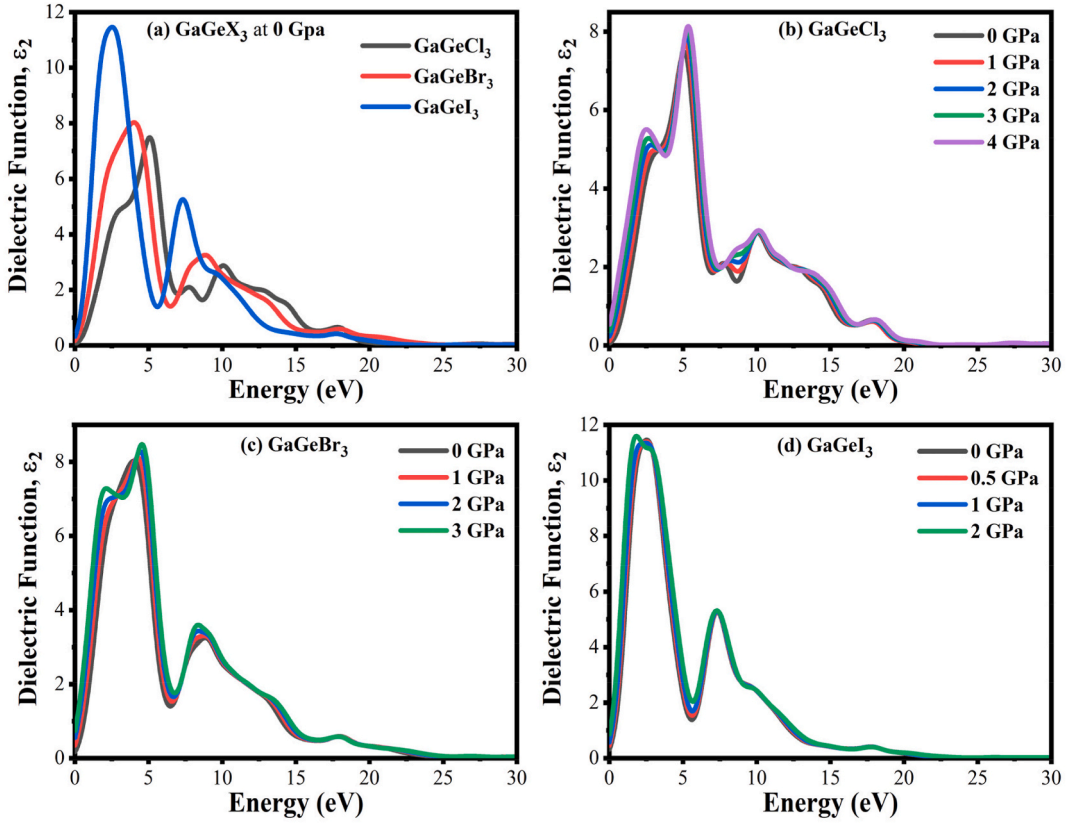

Fig. 7. Calculating how pressure affects the dielectric's imaginary component of $GaGeX_3$ (X = Cl, Br, and I) compounds.

work. A material's elevated static dielectric indicates reduced E_b (exciton binding energy) and lower charge carrier recombination rate [44]. For the momentum representation of matrix components in between electrical states that are occupied and vacant, the imaginary component (ε_2), of the complex dielectric function can be calculated utilizing the CASTEP-supported formula given as follows:

$$\varepsilon_2(\omega) = \frac{2e^2\pi}{\Omega\varepsilon_0}\sum_{k,v,c}\left|\psi_k^c\right|\widehat{U}\cdot\vec{r}\left|\psi_k^v\right|^2\delta\left(E_k^c - E_k^v - E\right)$$

In this work, we looked at how the dielectric function fluctuated at various pressures in all perovskite materials, including the real and imaginary components. The findings are shown in Figs. 6(a–d) and 7(a–d) with up to 30 eV. The dielectric function's imaginary part (ε_2) is directly associated with electron excitation, whereas the real part (ε_1) offers details about the electronic polarization of the material. The way a material responds to incoming light radiation determines the dielectric constant values [45]. The long-term execution of optoelectronic devices is significantly enhanced via lower charge carrier recombination rates, which are linked to higher dielectric ε_1 values. At 0 GPa, the compound is better suitable for application in optoelectronic devices when halogen Br and I are substituted for Cl, as shown by an increase in the value of ε_1 in the IR zone and a decreasing nature in the visible energy area. In the same way, the imaginary dielectric constant (ε_2) intensifies its shifting towards the low-energy region. Furthermore, there is greater absorption and bigger values of (ε_2) in the visible and early UV areas. In the visible and infrared zones, both dielectric values are higher for all perovskite materials, whereas they dropped in the ultraviolet.

Next, we looked at $GaGeX_3$'s pressure-induced dielectric function which is illustrated in Figs. 6(b–d) and 7(b–d). Pressure increases from 0 to 4 GPa, leading to an increase in the real component of the dielectric value in the region of low-energy of $GaGeCl_3$. The value of ε_1 is 10.3 for $GaGeCl_3$ at 0 eV when the pressure reaches 4 GPa and at energy levels above 0 eV, ε_1 declines. Next, it displays a negative value in the area with greater energy, suggesting that it is metallic. The ε_1 component in the region of low energy of the $GaGeBr_3$ and $GaGeI_3$ materials is seen in Fig. 6(c and d) to rise when the pressure is increased from 0 to 3 GPa for $GaGeBr_3$ and 0–2 GPa for $GaGeI_3$, respectively. The true dielectric value for the higher energy area does not significantly change as pressure rises for both but declines to negative.

Also, the value imaginary dielectric constant increases in the whole spectrum as pressure rises for all compounds. There are three notable (ε_2) peaks are seen in the low-energy area for $GaGeCl_3$ and $GaGeBr_3$ compounds. The first maximum peaks are at 2.46 eV and 2.05 eV; the second highest peaks are at 5.47 eV and 4.52 eV; the third maximum peaks are at 10.02 eV and 8.37 eV, respectively for $GaGeCl_3$ and $GaGeBr_3$ are depicted in Fig. 7(b and c). On the other hand, $GaGeI_3$ also has two significant imaginary peaks at 1.82 eV

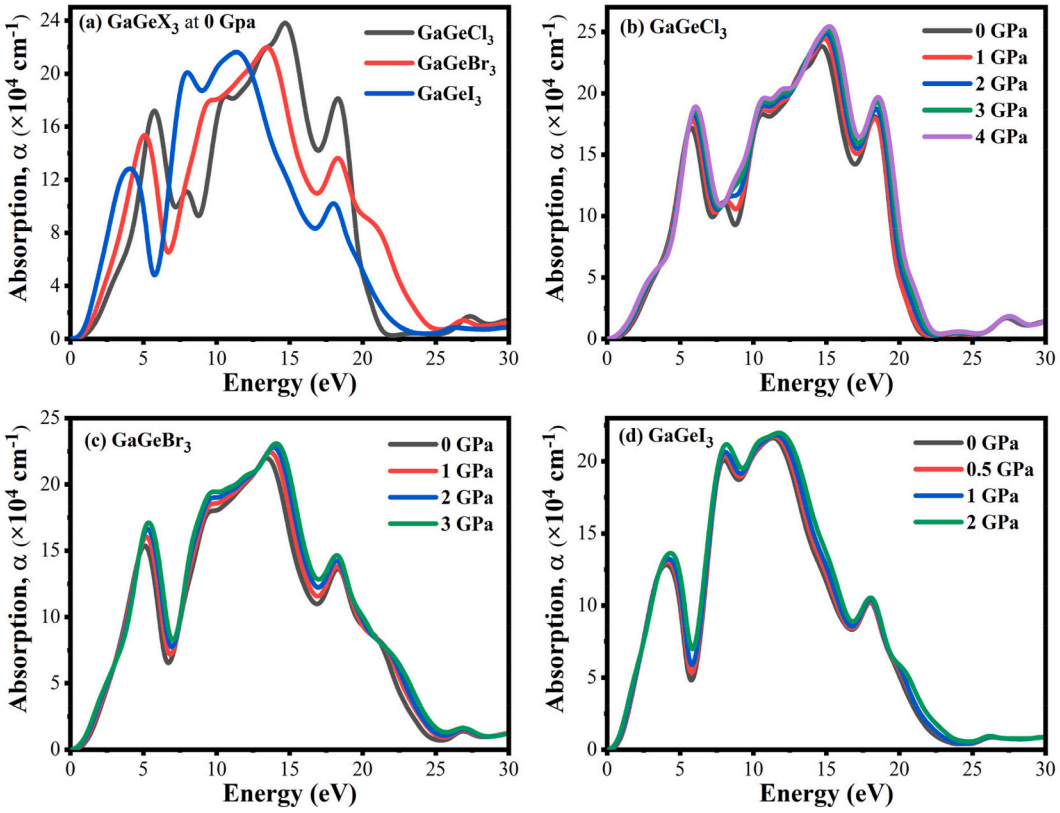

Fig. 8. Illustrated the absorption spectra of $GaGeX_3$ (where X = Cl, Br, and I) with energy under pressure.

and 7.33 eV which is shown in Fig. 7(d). Also, the value of ε_2 is higher for $GaGeI_3$ compared to other compounds. Then in the higher energy region, the value of ε_2 drops under pressures for all compounds.

Looking at both dielectric constants, it is clear that $GaGeI_3$ has a much bigger dielectric constant amplitude under pressure and without pressure contrasted with the other compounds in the visible area. As a result, both the E_b and the charge carrier recombination rate decrease. Thus, $GaGeI_3$ functions excellent for use in solar cell systems within the sector of photovoltaic.

The optical absorption coefficient, denoted as (α), quantifies the fraction of energy that a material absorbs per unit distance. It also affects the different optoelectronic devices' efficiency along with solar cells. It is only one of the many optical properties that have a big impact on performance [46]. The variation of α at 0 GPa with the energy of the photon is seen in Figs. 8(a) and 9(a). For each compound, there are four distinct peaks seen within the energy spectrum of 0–30 eV. $GaGeCl_3$ is shown to attain its greatest peak at 14.7 eV in Fig. 8(a). Conversely, the replacement of Cl for Br and I resulting a redshift; the highest peaks of $GaGeBr_3$ and $GaGeI_3$ are found at 13.5 eV and 11.4 eV, separately.

The difference in optical absorption of $GaGeX_3$ (X = Cl, Br, and I) perovskites when pressured, is illustrated in Fig. 8(b–d). In the visible range, $GaGeX_3$ exhibits pressure-induced band gap shifting, and its absorption edge moves to the area of low energy (redshift). Pressure significantly boosts the absorption edge of $GaGeX_3$, as displayed in Fig. 9(b–d) inside the visible region. However, the absorption of all compounds increased with blueshift at higher energy levels. In comparison to $GaGeBr_3$ and $GaGeI_3$ perovskites, $GaGeCl_3$ material exhibits the highest value of absorption in the ultraviolet region (ranging from 14.7 eV to 15.2 eV). The band gap for the energy of $GaGeX_3$, which is uniform with the absorption in the visible region, is as follows: E_g ($GaGeCl_3$) > E_g ($GaGeBr_3$) > E_g ($GaGeI_3$). Furthermore, as per Fig. 9(a–d), $GaGeI_3$ is the material with the highest absorption efficiency out of the three in the visible area. It implies that $GaGeI_3$ is a superior option to the other two when it comes to solar cell material. Because of their high absorption coefficients, all compounds are generally suitable for using multijunction solar cells.

The photoconductivity (σ) of a substance is a measure of how many photons it can transmit. The spectrum of conductance of $GaGeX_3$ (X = Cl, Br, and I) at 0 GPa are presented in Figs. 10(a) and 11(a). The absorption patterns of $GaGeX_3$ and these spectra resemble one other since these are derived from above. In the visible spectrum, $GaGeI_3$ exhibits higher photoconductivity, at about 3.95 fs^{-1}, compared to 3.44 fs^{-1} and 2.21 fs^{-1} for $GaGeBr_3$ and $GaGeCl_3$, respectively, as shown in Fig. 11(a). When Cl is replaced by the heavy halogens (Br and I), a redshift occurs. Each compound has two prominent peaks within the energy band at 0–30 eV.

$GaGeX_3$ (X = Cl, Br, and I) perovskites' pressure-dependent conductivity is shown in Figs. 10(b–d) and 11(b–d). Increased pressure leads to improved conductivity. A change in the conductivity edge toward the low-energy zone is brought about by the applied pressure. High energy levels and increased pressure cause a blueshift of conductivity peaks. To make things simpler to implement, Fig. 11(b–d) shows the conductivity in the visible area under applied pressure. With applied pressure, the perovskite containing I

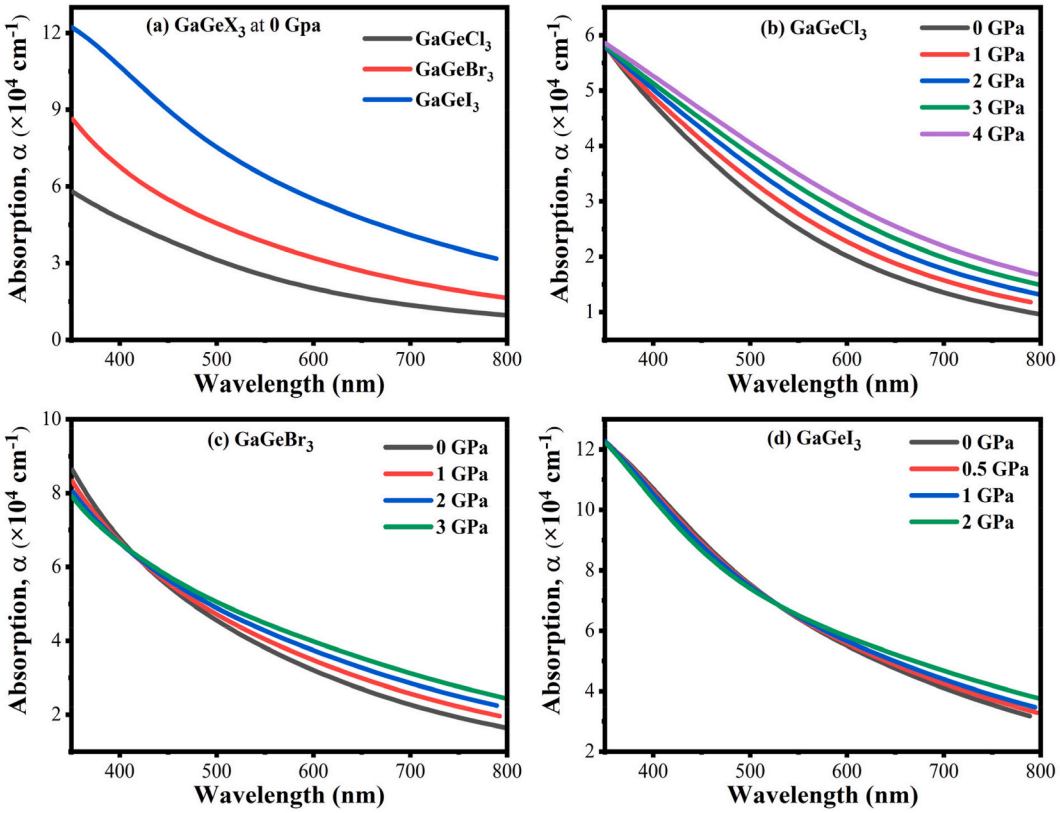

Fig. 9. Pressure-induced optical absorption of $GaGeX_3$ concerning wavelength, where X is equal to Cl, Br, and I.

exhibits superior conductivity in the visible region when compared to Cl and Br. Conductivity peaks in the higher energy area are blue-shifted as seen in Fig. 10(b–d). The conductivity value range is σ ($GaGeI_3$) > σ ($GaGeBr_3$) > σ ($GaGeCl_3$). Throughout the whole spectrum, materials made of $GaGeX_3$ have certain conductivity peaks. These peaks, with the largest peak at 5.26 eV, are seen in $GaGeCl_3$ at 5–5.5 eV and 9.5–10.5 eV ranges at different pressures. Consequently, $GaGeBr_3$ exhibits notable peaks at 4.5–5 eV and 8.5–9.5 eV, separately, with 4.47 eV being the largest peak. On the other hand, $GaGeI_3$ holds two primary peaks, located at 2.5–3.5 eV and 7–8 eV, respectively. Also, $GaGeI_3$ has the highest intensity peak occurring at 7.44 eV.

Fig. 12(a) illustrates the reflectivity spectra of the substances under investigation, which helps to know about the topology of compounds. Solar efficiency is reduced when there is more reflection in the spectrum of visible light. Fig. 12(a) shows the reflectance (R) of $GaGeX_3$ (X = Cl, Br, and I) at 0Gpa. At 0 eV, $GaGeCl_3$ has a very low reflectance of around 0.22, as seen in Fig. 12(a). Nevertheless, when Cl is replaced with Br and I, respectively, the reflectance for $GaGeBr_3$ and $GaGeI_3$ increases to 0.27 and 0.34. Fig. 12(a) further demonstrates that in the visible range, $GaGeX_3$ (X = Cl, Br, and I) exhibits increased reflectivity, whereas $GaGeI_3$ has the highest level. The solar material's utility is diminished by $GaGeI_3$'s elevated optical reflection. Hence, more research is required to enhance the photovoltaic efficiency of $GaGeI_3$ and decrease its reflectance.

The reflectivity that varies with pressure is seen in Fig. 12 (b–d). Based on these figures, the reflectivity spectra undergo a redshift at low energy, and then a blueshift at high energy as a result of applied pressure, respectively. But for any compound, the rise in reflectivity value is negligible. Throughout the whole spectrum, $GaGeX_3$ materials display some peaks when subjected to pressure. Approximately at 2.12 eV, the first absorption peak for $GaGeCl_3$ was observed. In addition, additional peaks were noted for the following compounds: $GaGeCl_3$ at about 6.2 eV, 10.6 eV, 16.1 eV, and 19.5 eV; $GaGeBr_3$ at 1.46 eV, 5.43 eV, 9.57 eV, 15 eV, and 18.7 eV; and $GaGeI_3$ at 1.38 eV, 3.77 eV, 8.34 eV, 13.2 eV, and 18.5 eV. The low reflectivity of all materials throughout the spectrum, especially in the visible area, may be advantageous for the applications of solar cells due to their considerable absorptivity. According to Fig. 12(a–d), $GaGeX_3$ compounds have excellent reflectivity within the UV region, suggesting that they might be used as coating materials to mitigate solar heating in this electromagnetic spectrum. In addition, $GaGeI_3$'s larger UV reflectance spectrum makes it an attractive candidate for UV shielding applications.

The refractive index spectrum at 0 GPa is depicted in Fig. 13(a). It clearly shows a decreasing trend with increasing light energy, with the highest peak taking place at 0 eV. Fig. 13(a) further shows that $GaGeCl_3$ has a static refractive index of 2.72. The trend indicates an upward movement from Cl to I, with $GaGeBr_3$ reaching 3.11 and $GaGeI_3$ reaching 3.7, respectively. The infrared area of the compounds has the greatest refractive index, but the lowest in the UV portion. Among the compounds, $GaGeI_3$ is most suited for waveguide applications due to its high refractive index at 0 eV [47].

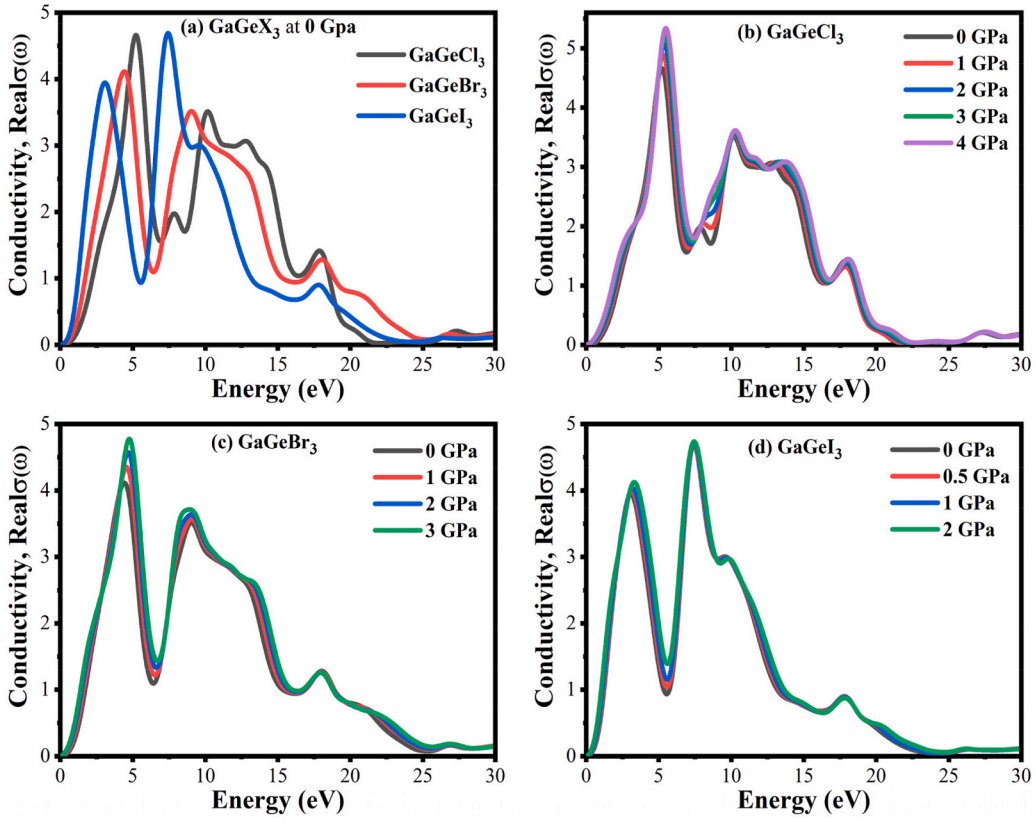

Fig. 10. Exploring the conductivity spectra of $GaGeX_3$ compounds (X = Cl, Br, and I) with energy.

The refractive index of $GaGeX_3$ (X = Cl, Br, and I) perovskites with applied pressure is presented in Fig. 13 (b–d). Under applied pressure, the refractive values of all substances are increased in the low-energy area. All studied materials have the maximum refractive value at 0 eV. In regions of higher energy, the refractive index of $GaGeCl_3$ may reduce and even blueshift sometimes. However, in the higher energy range, there are no notable changes in the refractive index for $GaGeBr_3$ and $GaGeI_3$ materials. In the visible area, the refractive index of any substance is minimal. Solar cells and other optoelectronic applications benefit from these materials for that reason.

With no crystallographic distortion of the materials, we now know that semiconductors emerged as conductors when pressure was applied, and that this overlapping of CB and VB is the reason why $GaGeX_3$ (X = Cl, Br, and I) perovskites improved their optical and electronic properties. Because hydrostatic pressure may be used to tune the characteristics of any compound. In this study, the materials we studied have great potential as solar cells, UV absorbers, waveguide applications, and other optoelectronic devices.

3.4. Mechanical properties

In order to estimate elastic constants, it is necessary to calculate the stress tensor for a diversity of deformed structures. With the help of the CASTEP Elastic Constants task, we can get the full 6 × 6 tensor of elastic constants for any symmetric three-dimensional periodic structure. For assessing the mechanical stability of compounds, a table of elastic constants (C_{ij}) is provided in Tables S3–S5 [48]. Conditions for Born stability are met by all three elastic constants for $GaGeX_3$ (X = Cl, Br, and I) under investigation when pressure is applied [49], where three main components are C_{11}, C_{12}, C_{44} denoting longitudinal stiffness, off-diagonal stiffness, and shear stiffness respectively.

$C_{11} > 0$; $C_{44} > 0$; $C_{11} > C_{12}$

$C_{11} + 2C_{12} > 0$; $C_{12} < B < C_{11}$

According to the Voigt, Reuss, and Hill schemes, the output comprises the averages of Young's, the bulk, and the shear modulus, along with Poisson's ratio. In relation to the corresponding single-crystal properties, the VRH approximation provides practical values for the elastic moduli with polycrystalline crystal. The Voigt and Reuss bulk modulus (B), shear modulus (G), and Pugh's ratio are expressed as [50],

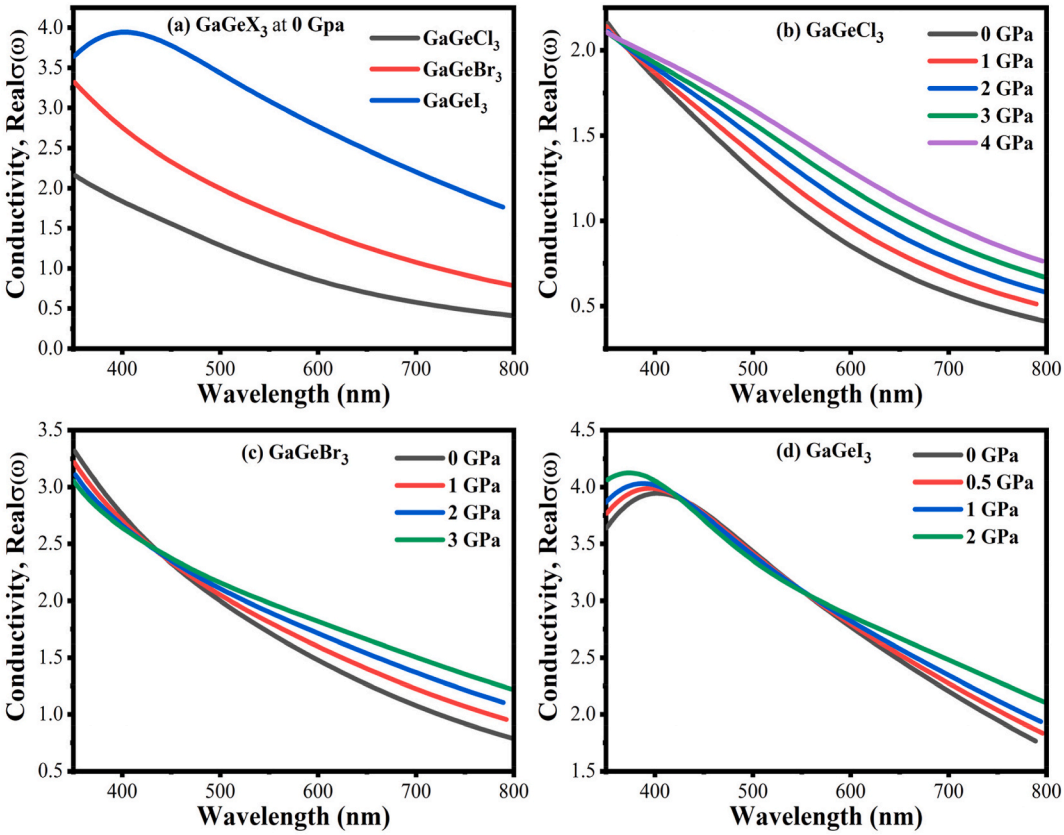

Fig. 11. Exploring the variations in conductivity at different wavelengths while studying the effects of different pressures on $GaGeX_3$ compounds (with X being Cl, Br, and I).

$$B_V = B_R = 1/3\ \ (C_{11} + 2C_{12}) \tag{2}$$

$$G_R = \frac{5(C_{11} - C_{12})C_{44}}{3(C_{11} - C_{12}) + 4C_{44}} \tag{3}$$

$$G_v = 1/5\ \ (C_{11} - C_{12} + 3C_{44}) \tag{4}$$

The final shear modulus and bulk modulus are calculated by [51],

$$B = \frac{1}{2}(B_v + B_R) \tag{5}$$

$$G = \frac{1}{2}\ G_v + G_R \tag{6}$$

By utilizing B and G, we derived the average the Poisson's ratio ν and Young's modulus E, thereby facilitating comprehension of mechanical properties in the context of DFT calculations [48],

$$\text{Young Modulus}, E = \frac{9BG}{3B + G} \tag{7}$$

$$\text{Poisson ratio}, \nu = \frac{(3B\text{-}2G)}{2(3B + G)} \tag{8}$$

$$\text{Pugh's ration} = B/G \tag{9}$$

$$\text{Machinability index}, \mu_m = B/C_{44} \tag{10}$$

The subsequent hardness of $GaGeX_3$ (X = Cl, Br, I) is computed utilizing Tian's model [52],

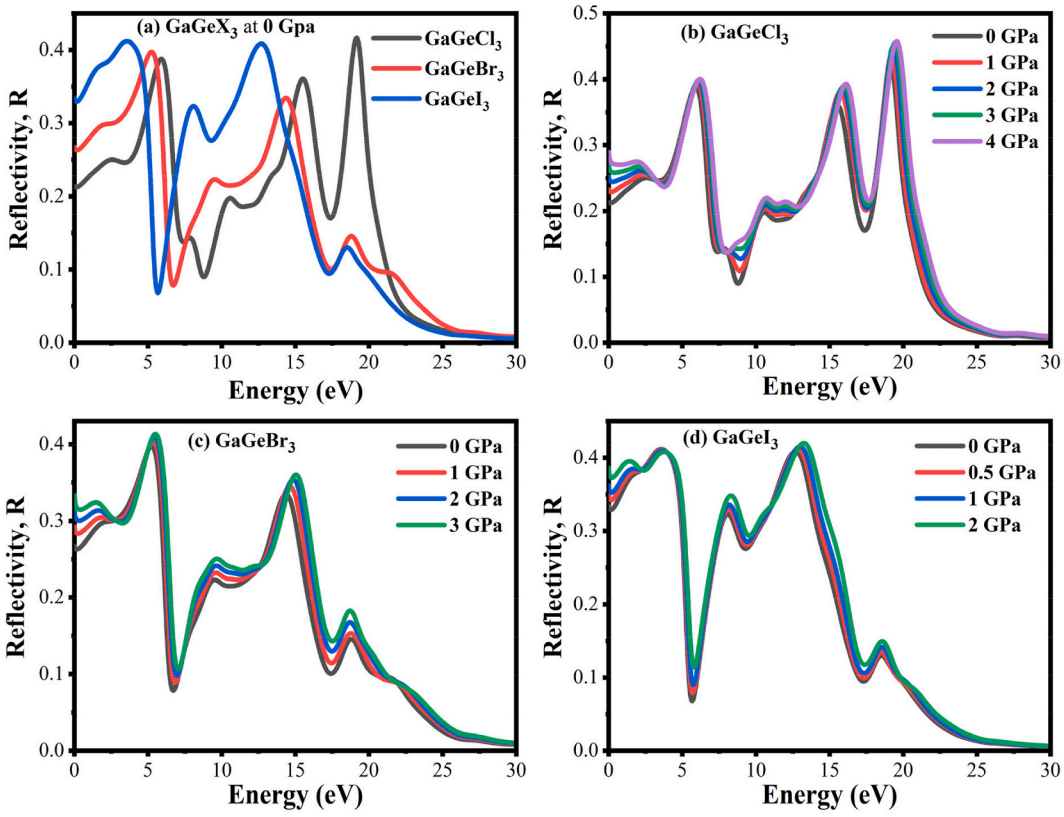

Fig. 12. The optical reflectivity of $GaGeX_3$ (where X = Cl, Br, and I) induces by pressure.

$$H_{v,Tian} = 0.92\, K^{1.137} G^{0.708} \tag{11}$$

Here, K = B/G.

The data from Tables S3(a), S4(a), and S5(a) indicate that the elastic constant C_{ij} rises as pressure increases, but C_{44} is less affected by hydrostatic pressure. The fluctuation of elastic constants is depicted in Fig. 14 with different pressures. The Cauchy pressure (C_{12}–C_{44}) is a crucial measure of a material's ductility or brittleness. When this characteristic has a negative value, it signifies that the material is brittle. Conversely, a positive value suggests the ductility of a material. The ductile behavior of $GaGeX_3$ is reflected according to the positive Cauchy pressure in Tables S3(a), S4(a), and S5(a). Furthermore, as pressure increases, the ductility of these compounds increases except $GaGeBr_3$ as shown in Fig. 16. However, an examination of the $GaGeBr_3$ reveals that the Cauchy pressure decreases when pressure increases, which reveals a reduction in the number of void spaces between particles. The subsequent increase in Cauchy pressure is due to the material reaching a critical density, at which point its resistance to compression diminishes.

The changes in shear, bulk, and Young's modulus of $GaGeX_3$ (where X is equal to Cl, Br, and I) under pressure are illustrated in Fig. 15. From Fig. 15, it is clear that the bulk modulus value for $GaGeCl_3$ increases when pressure increases, denoting more resistance to external deformation and is stiffer compared to non-pressurized states. The same result was also found for $GaGeI_3$ leading to close-packed atoms. However, the fact that the $GaGeBr_3$'s bulk modulus decreases initially with increasing pressure (up to 1 GPa) suggests that atomic bond interactions may change slightly; however, as pressure increases above 1 GPa, B increases again, also increasing plastic deformation resistance. The material's shear modulus (G) also denotes its fracture resistance. The G values of $GaGeX_3$ (X = Cl, Br, and I) are increasing linearly with increasing pressure which is aligned with Fig. 15 and Tables S3(a), S4(a) and S5(a). But if we compare B and G among the three compounds at 2 GPa, $GaGeCl_3$ shows better values of B and G. Consequently, materials with higher E values are associated with greater stiffness. E increases linearly as the pressure increases for $GaGeX_3$ (X = Cl, Br, I) perovskites. Since pressure is increased, $GaGeCl_3$ exhibits the greatest rigidity among the three perovskites.

If the ratio of B to G is more than 1.75, the material exhibits ductile behavior; otherwise, it exhibits brittle behavior [53]. All three compounds show ductile nature at both pressurized and non-pressurized states according to Tables S3(a), S4(b), and S5(c). The variety in Cauchy pressure, Pugh's, and Poisson's ratio of cubic $GaGeX_3$ (X = Cl, Br, and I) at varying pressures are displayed in Fig. 16. Here, the Pugh's ratio increases when pressure increases for $GaGeI_3$ and $GaGeCl_3$ but for $GaGeBr_3$ initially decreases at 1 GPa, followed by a slight increase. The Poisson's ratio for ductility is above 0.26 [54]. From this point of view, all the compounds have Poisson's ratio above this value. This situation is evident in the ductile behavior of all compounds.

The $GaGeCl_3$'s hardness decreases under applied pressure, consequently machinability index increases as in Table S3(a). The machinability index reflects a material's ability to be shaped and its lubricating characteristics. As a result of applying pressure, the

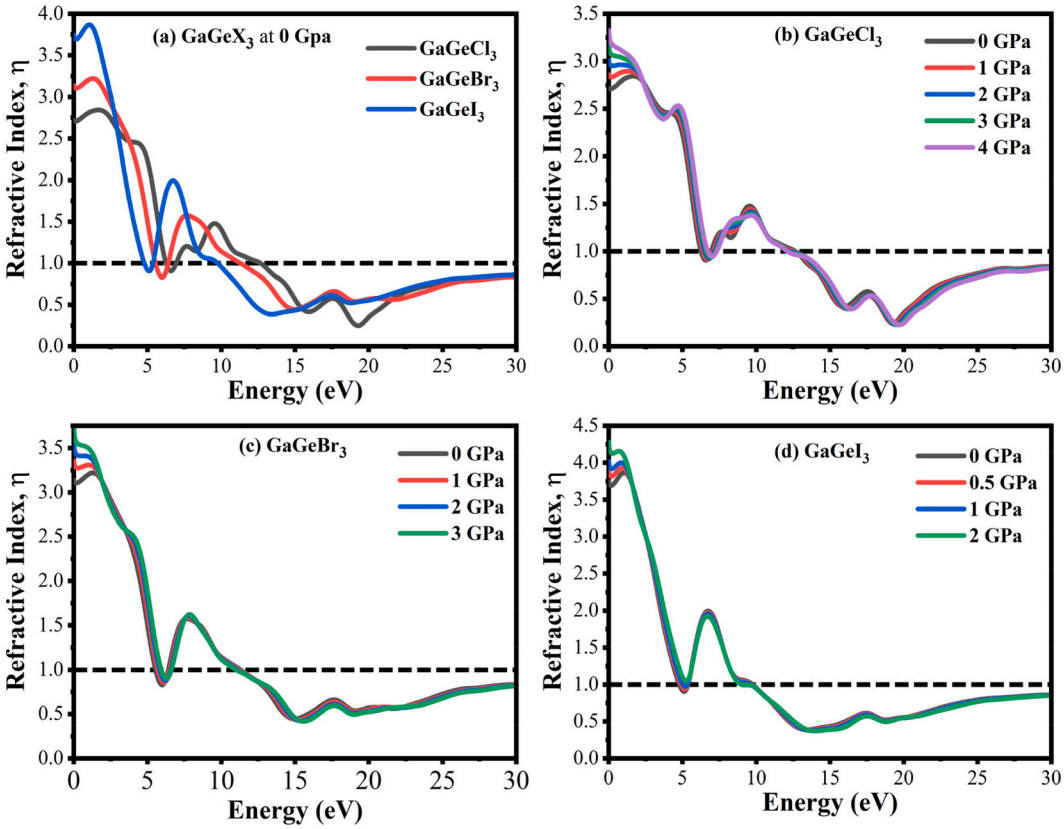

Fig. 13. Exploring the refractive index of $GaGeX_3$ (X = Cl, Br, and I) with applied pressure.

machinability of $GaGeCl_3$ is significantly increased which is attributed to the reduction in hardness, which results in improved lubricity properties. The hardness of $GaGeBr_3$ and $GaGeI_3$ at ambient pressure show non-linear nature as shown in Fig. 17. But both $GaGeBr_3$ and $GaGeI_3$ exhibit improved machinability at increasing pressure, identical to $GaGeCl_3$. The machinability of $GaGeCl_3$ was found to be superior among the three perovskites.

One approach to assess the directional variability of a system's attributes is to use the anisotropic index. When assessing the atomic bond strength's degree of anisotropy across several crystallographic planes, including {100}, {010}, and {001}, the shear anisotropy factor in cubic systems is useful. Three shear anisotropy factors (A_1, A_2, and A_3) for these planes are computed using a particular equation [55].

$$A_1 = A_2 = A_3 = \frac{4C_{44}}{C_{11} + C_{33} - 2C_{13}} \tag{12}$$

A similar expression for the Zener anisotropy factor (A) follows [56].

$$A = \frac{2C_{44}}{C_{11} - C_{12}} \tag{13}$$

Anisotropy indicates a departure from unity in isotropic materials, where A = 1 [56]. Tables S3(b), S4(b), and S5(b) show that the $GaGeX_3$'s (X = Cl, Br, and I) elastic anisotropy has increased at increasing pressures. For different crystal planes, it is preferable to use a single anisotropy index rather than several components to more easily capture this anisotropy. Chung and Buessem also determined the anisotropy percentage using an empirical method in both shear and bulk [57]. Elastic isotropy is shown when A_B and A_G equals zero. However, both the pressurized and non-pressurized conditions show that the computed values of A_B and A_G are non-zero. This indicates that all $GaGeX_3$ (where X = Cl, Br, and I) are anisotropic. The fact that the universal anisotropy factor (A^U), which Ranganathan and Ostoja-Starzewski initially proposed, may be used for any crystal symmetry makes it very attractive. A^U is 0 for isotropic materials [58]. Tables S3(b), S4(b), and S5(b) emphasize that the substances under study have elastic anisotropy, with anisotropy increasing significantly with pressure. To demonstrate the directional dependence of elastic characteristics in $GaGeX_3$ perovskites, 3D anisotropic contour plots for E, G, and υ were created and shown in Figs. S7–9. The deviation found in these contour plots from the spherical shape indicates the anisotropic nature of the perovskites under investigation [41]. Pressure exerts a significant impact on the directional elasticity of $GaGeX_3$ perovskites, as evidenced by the sharp rise in anisotropy when pressure increases from 0 GPa up to 4 GPa.

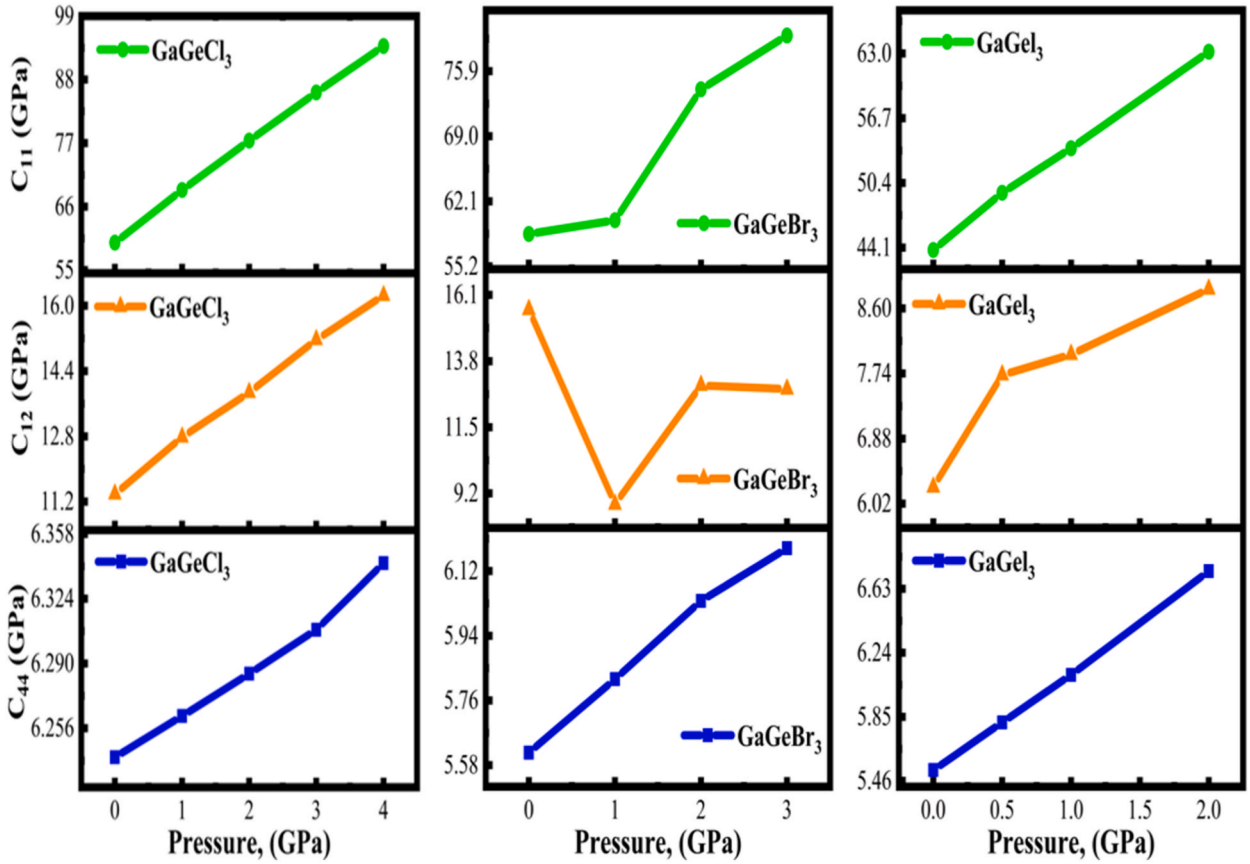

Fig. 14. Elastic constants of C_{11}, C_{12}, and C_{44} for $GaGeX_3$ (X = Cl, Br, and I) vary with pressure.

4. Conclusion

In conclusion, exploring the effects of hydrostatic pressures on material properties is an intriguing area of study. Applying pressure to compounds like $GaGeX_3$ (X = Cl, Br, and I) can modify their electronic structure, bandgap, and other important properties. This flexibility allows for a variety of useful applications such as solar cells and different optoelectronic devices. Based on the born stability criterion, all perovskites are stable mechanically under applied pressure. Positive Cauchy pressure and Pugh's ratio exhibit ductile behavior of all investigated compounds. These perovskite materials have low bulk modulus that's why these are ideal for thin-layer fabrication. They also experience increasing shear and Young's modulus as increasing pressure. $GaGeCl_3$, the stiffest of the three perovskites, exhibits the most marked rigidity under pressure. The substantial enhancement in machinability of $GaGeX_3$ resulting a decrease in hardness under pressure, which in turn leads to enhanced lubricity characteristics. In addition, these substances possess important mechanical properties: anisotropy, ductility, and mechanical stability, which are further enhanced when subjected to pressure. When subjected to positive hydrostatic pressure, the lattice parameter experiences a decrease, resulting in a more negative formation energy that reveals their thermodynamic stability. Also, the decreasing nature of bond length under pressure makes stronger bonding between atoms. These attributes are crucial for the development of multi-junctional solar cells and high-performance optoelectronic devices. The band gap values are calculated with PBE along with HSE06 potentials that exhibit the direct band gap and semiconducting character of each compound. The metallic transition takes place after a certain pressure is applied. The participation of atoms in the VB and CBs can be determined from TDOS and PDOS, respectively. In the VBs, various orbitals such as Ga-4s, Cl-3p, Br-4p, and I-5p are involved. On the other hand, the conduction bands involve Ga-4p and Ge-4p orbitals. After investigation of optical properties, these materials became more viable for optoelectronic applications, both pressure and non-pressure conditions. In addition, our research reveals that all compounds exhibit higher values of (ε_2) and greater absorption in the visible and early UV regions. When comparing the three compounds, however, it becomes evident that $GaGeI_3$ has a significantly larger dielectric constant amplitude under pressure and without pressure in the visible range (1.8 eV and 7.33 eV) than the other two samples. This characteristic renders $GaGeI_3$ particularly well-suited for solar cell applications. However, $GaGeCl_3$ exhibits stronger absorption in the UV region (ranging from 14.7 eV to 15.2 eV). So, it is evident that $GaGeCl_3$ is a superior absorber of UV radiation. In addition, $GaGeI_3$ exhibited higher reflectivity when subjected to pressure making them suitable for UV shielding application. Regarding the refractive index, all three compounds exhibit a minimum value in the lower energy range, which is advantageous for optoelectronic applications.

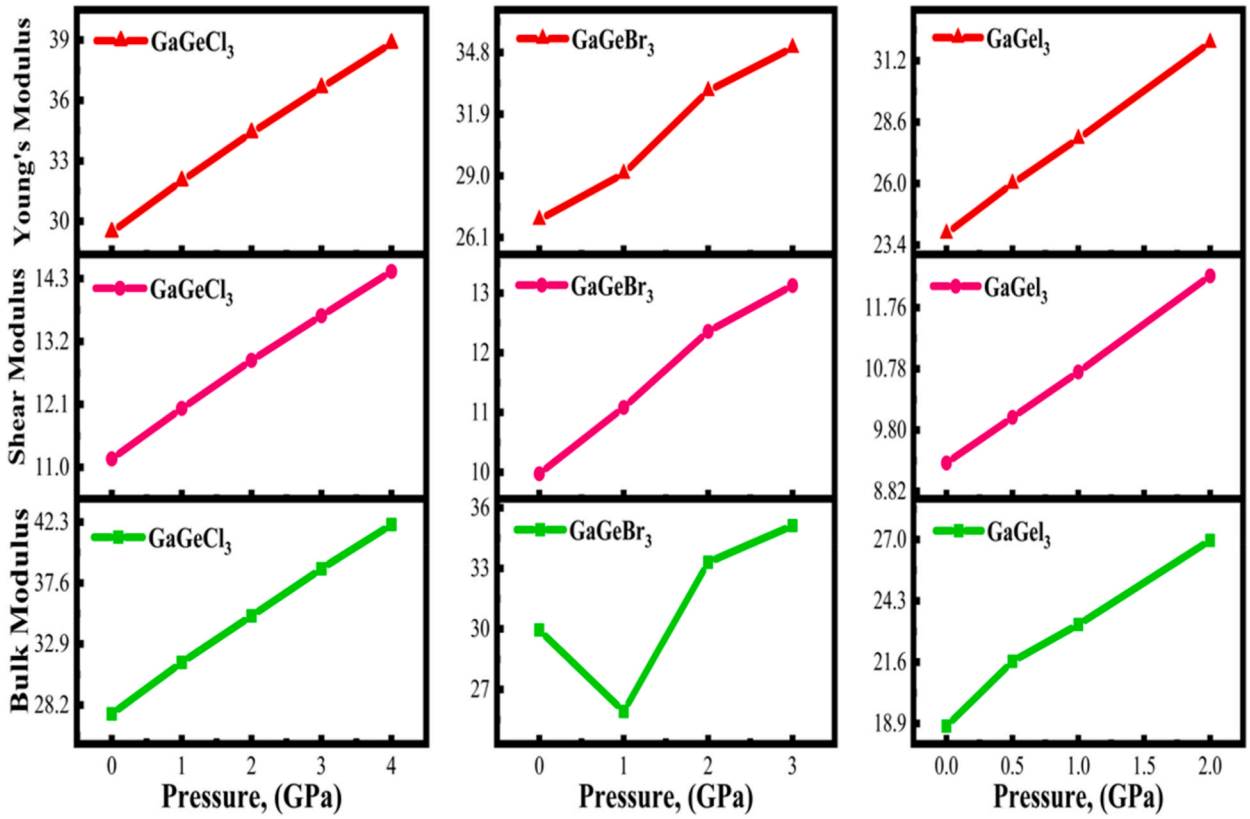

Fig. 15. Investigating the Young's, Shear, and Bulk Modulus of $GaGeX_3$ (X = Cl, Br, and I) with variation of pressure.

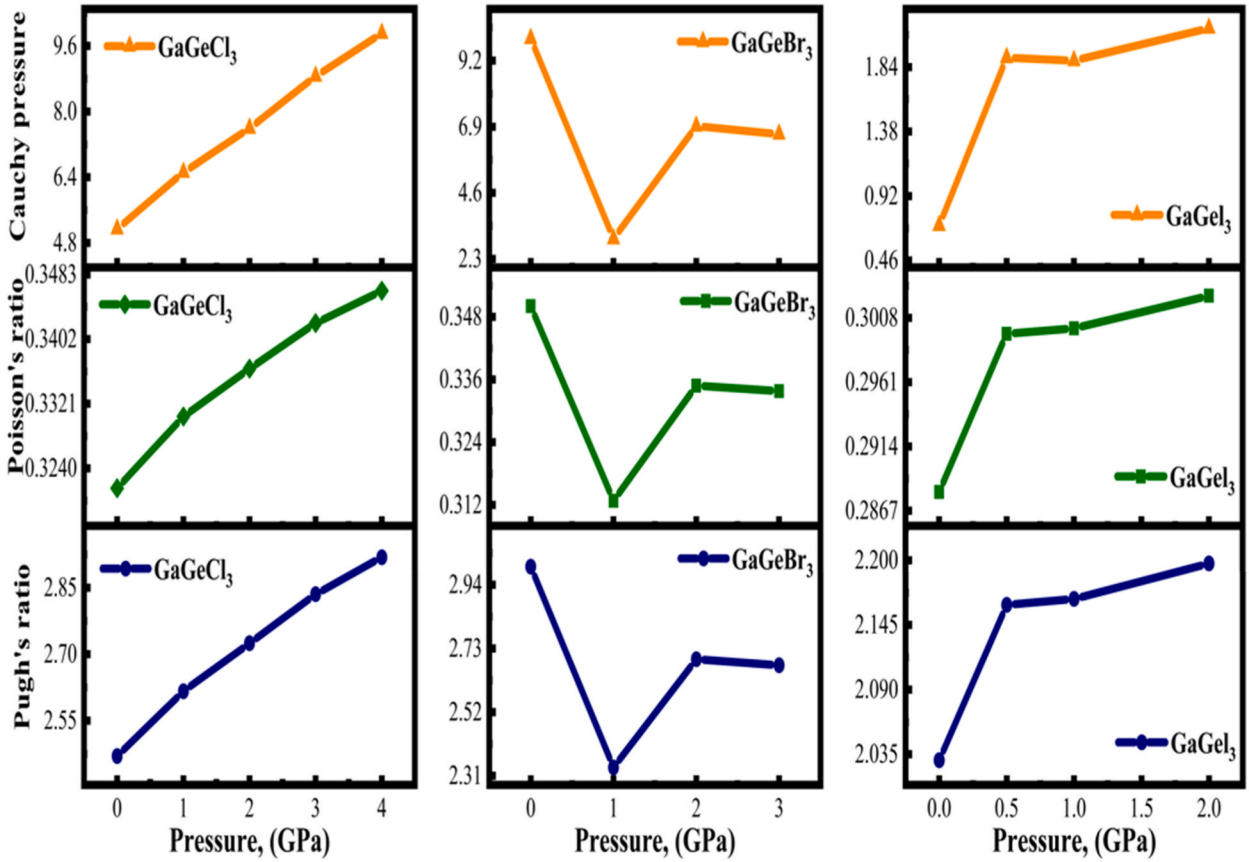

Fig. 16. Examining the changes in Cauchy pressure, Pugh's, and Poisson's ratio of cubic $GaGeX_3$ (X = Cl, Br, and I) at different pressures.

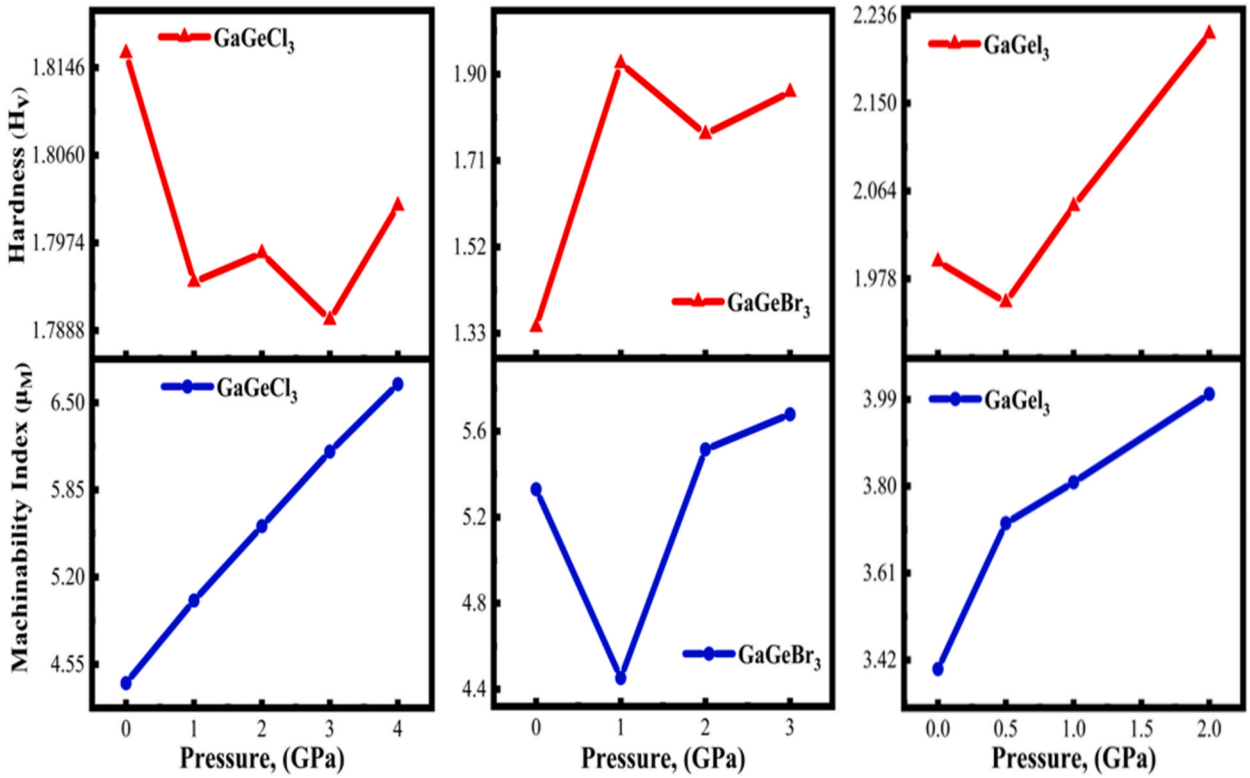

Fig. 17. Investigating the impact of pressure on the hardness and machinability index of $GaGeX_3$ (X = Cl, Br, and I).

CRediT authorship contribution statement

Md. Mehedi Hasan: Data curation, Formal analysis, Software, Writing – original draft. **Md. Amran Sarker:** Conceptualization, Data curation, Formal analysis, Investigation, Software, Writing – original draft. **Mohshina Binte Mansur:** Data curation, Formal analysis, Methodology, Writing – original draft. **Md. Rasidul Islam:** Conceptualization, Investigation, Resources, Supervision, Validation, Writing – review & editing. **Sohail Ahmad:** Funding acquisition, Project administration, Resources, Validation, Writing – review & editing.

Declaration of competing interest

The authors declare that they have no known competing financial interests or personal relationships that could have appeared to influence the work reported in this paper.

Acknowledgments

The authors extend their appreciation to the Deanship of Research and Graduate Studies at King Khalid University for funding this work through Large Research Project under grant number RGP2/415/45.

Appendix A. Supplementary data

Supplementary data to this article can be found online at https://doi.org/10.1016/j.heliyon.2024.e34824.

References

[1] H.S. Jung, N. Park, Perovskite solar cells: from materials to devices, Small 11 (2015) 10–25, https://doi.org/10.1002/smll.201402767.
[2] P.P. Boix, K. Nonomura, N. Mathews, S.G. Mhaisalkar, Current progress and future perspectives for organic/inorganic perovskite solar cells, Mater. Today 17 (2014) 16–23, https://doi.org/10.1016/j.mattod.2013.12.002.
[3] J.-P. Correa-Baena, M. Saliba, T. Buonassisi, M. Grätzel, A. Abate, W. Tress, A. Hagfeldt, Promises and challenges of perovskite solar cells, Science 358 (2017) 739–744, https://doi.org/10.1126/science.aam6323.

[4] I. Hussain, H.P. Tran, J. Jaksik, J. Moore, N. Islam, M.J. Uddin, Functional materials, device architecture, and flexibility of perovskite solar cell, Emergent Mater 1 (2018) 133–154, https://doi.org/10.1007/s42247-018-0013-1.

[5] M.A. Green, A. Ho-Baillie, H.J. Snaith, The emergence of perovskite solar cells, Nat. Photonics 8 (2014) 506–514, https://doi.org/10.1038/nphoton.2014.134.

[6] M. Solayman, M.R. Islam, M.A. Sarker, R.K. Sharme, M. Al Momin, M.R. Islam, A.A. Khan, A deep dive into structural, electronic, optical, and mechanical properties of ATiO $_3$ (A = Ba, Th): DFT insights, Phys. Scr. 98 (2023) 125944, https://doi.org/10.1088/1402-4896/ad0a27.

[7] A.M. Humada, M. Hojabri, S. Mekhilef, H.M. Hamada, Solar cell parameters extraction based on single and double-diode models: a review, Renew. Sustain. Energy Rev. 56 (2016) 494–509, https://doi.org/10.1016/j.rser.2015.11.051.

[8] T.D. Lee, A.U. Ebong, A review of thin film solar cell technologies and challenges, Renew. Sustain. Energy Rev. 70 (2017) 1286–1297, https://doi.org/10.1016/J.RSER.2016.12.028.

[9] M.K. Hossain, S. Bhattarai, A.A. Arnab, M.K.A. Mohammed, R. Pandey, M.H. Ali, MdF. Rahman, MdR. Islam, D.P. Samajdar, J. Madan, H. Bencherif, D. K. Dwivedi, M. Amami, Harnessing the potential of CsPbBr $_3$ -based perovskite solar cells using efficient charge transport materials and global optimization, RSC Adv. 13 (2023) 21044–21062, https://doi.org/10.1039/D3RA02485G.

[10] Y. Sun, W. Zhang, H. Chi, Y. Liu, C.L. Hou, D. Fang, Recent development of graphene materials applied in polymer solar cell, Renew. Sustain. Energy Rev. 43 (2015) 973–980, https://doi.org/10.1016/j.rser.2014.11.040.

[11] MdR. Islam, Y. Wu, K. Liu, Z. Wang, S. Qu, Z. Wang, Recent progress and future prospects for light management of all-perovskite tandem solar cells, Adv. Mater. Interfaces 9 (2022), https://doi.org/10.1002/admi.202101144.

[12] R. Padmavathy, A. Amudhavalli, M. Manikandan, R. Rajeswarapalanichamy, K. Iyakutti, A.K. Kushwaha, Electronic and optical properties of CsSnI3−yCly (y = 0, 1, 2, 3) perovskites: a DFT study, J. Electron. Mater. 48 (2019) 1243–1251, https://doi.org/10.1007/s11664-018-06850-8.

[13] G.E. Eperon, G.M. Paternò, R.J. Sutton, A. Zampetti, A.A. Haghighirad, F. Cacialli, H.J. Snaith, Inorganic caesium lead iodide perovskite solar cells, J. Mater. Chem. A Mater. 3 (2015) 19688–19695, https://doi.org/10.1039/C5TA06398A.

[14] J. Li, Z. Han, Y. Gu, D. Yu, J. Liu, D. Hu, X. Xu, H. Zeng, Perovskite single crystals: synthesis, optoelectronic properties, and application, Adv. Funct. Mater. 31 (2021), https://doi.org/10.1002/adfm.202008684.

[15] L. Chouhan, S. Ghimire, C. Subrahmanyam, T. Miyasaka, V. Biju, Synthesis, optoelectronic properties and applications of halide perovskites, Chem. Soc. Rev. 49 (2020) 2869–2885, https://doi.org/10.1039/C9CS00848A.

[16] W. Zhang, G.E. Eperon, H.J. Snaith, Metal halide perovskites for energy applications, Nat. Energy 1 (2016) 16048, https://doi.org/10.1038/nenergy.2016.48.

[17] W. Yin, T. Shi, Y. Yan, Unique properties of halide perovskites as possible origins of the superior solar cell performance, Adv. Mater. 26 (2014) 4653–4658, https://doi.org/10.1002/adma.201306281.

[18] R. Padmavathy, A. Amudhavalli, R. Rajeswarapalanichamy, K. Iyakutti, Electronic and optical properties of cubic perovskites $CsPbCl_{3-y}I_y$ (y = 0, 1, 2, 3), Z. Naturforsch. 74 (2019) 905–913, https://doi.org/10.1515/zna-2018-0516.

[19] W.S. Yang, B.-W. Park, E.H. Jung, N.J. Jeon, Y.C. Kim, D.U. Lee, S.S. Shin, J. Seo, E.K. Kim, J.H. Noh, S. Il Seok, Iodide management in formamidinium-lead-halide–based perovskite layers for efficient solar cells, Science 356 (2017) 1376–1379, https://doi.org/10.1126/science.aan2301.

[20] K. Nishimura, M.A. Kamarudin, D. Hirotani, K. Hamada, Q. Shen, S. Iikubo, T. Minemoto, K. Yoshino, S. Hayase, Lead-free tin-halide perovskite solar cells with 13% efficiency, Nano Energy 74 (2020) 104858, https://doi.org/10.1016/j.nanoen.2020.104858.

[21] Y. Yuan, R. Xu, H.-T. Xu, F. Hong, F. Xu, L.-J. Wang, Nature of the band gap of halide perovskites ABX_3 (A = CH_3 NH_3, Cs; B = Sn, Pb; X = Cl, Br, I): first-principles calculations, Chin. Phys. B 24 (2015) 116302, https://doi.org/10.1088/1674-1056/24/11/116302.

[22] M. Roknuzzaman, K. Ken Ostrikov, K. Chandula Wasalathilake, C. Yan, H. Wang, T. Tesfamichael, Insight into lead-free organic-inorganic hybrid perovskites for photovoltaics and optoelectronics: a first-principles study, Org. Electron. 59 (2018) 99–106, https://doi.org/10.1016/j.orgel.2018.04.051.

[23] T.A. Berhe, W.-N. Su, C.-H. Chen, C.-J. Pan, J.-H. Cheng, H.-M. Chen, M.-C. Tsai, L.-Y. Chen, A.A. Dubale, B.-J. Hwang, Organometal halide perovskite solar cells: degradation and stability, Energy Environ. Sci. 9 (2016) 323–356, https://doi.org/10.1039/C5EE02733K.

[24] M. Coduri, T.B. Shiell, T.A. Strobel, A. Mahata, F. Cova, E. Mosconi, F. De Angelis, L. Malavasi, Origin of pressure-induced band gap tuning in tin halide perovskites, Mater. Adv. 1 (2020) 2840–2845, https://doi.org/10.1039/D0MA00731E.

[25] M.I. Kholil, M.T.H. Bhuiyan, Effects of pressure on narrowing the band gap, visible light absorption, and semi-metallic transition of lead-free perovskite CsSnBr3 for optoelectronic applications, J. Phys. Chem. Solid. 154 (2021) 110083, https://doi.org/10.1016/J.JPCS.2021.110083.

[26] S. Guo, Y. Zhao, K. Bu, Y. Fu, H. Luo, M. Chen, M.P. Hautzinger, Y. Wang, S. Jin, W. Yang, X. Lü, Pressure-suppressed carrier trapping leads to enhanced emission in two-dimensional perovskite (HA) $_2$ (GA)Pb $_2$ I $_7$, Angew. Chem. 132 (2020) 17686–17692, https://doi.org/10.1002/ange.202001635.

[27] Md Solayman, MdA. Sarker, M. Muntasir, R.K. Sharme, MdR. Islam, Pressure-induced investigation of structural, electronic, optical, and mechanical properties of BaCeO3, Opt. Mater. 148 (2024) 114699, https://doi.org/10.1016/j.optmat.2023.114699.

[28] MdF. Rahman, MdA.I. Islam, MdR. Islam, MdH. Ali, P. Barman, MdA. Rahman, Md Harun-Or-Rashid, M. Hasan, M.K. Hossain, Investigation of a novel inorganic cubic perovskite Ca $_3$ PI $_3$ with unique strain-driven optical, electronic, and mechanical properties, Nano Select. 4 (2023) 632–645, https://doi.org/10.1002/nano.202300066.

[29] MdA. Sarker, M.M. Hasan, Md Al Momin, A. Irfan, MdR. Islam, A. Sharif, Band gap engineering in lead free halide cubic perovskites GaGeX 3 (X = Cl, Br, and I) based on first-principles calculations, RSC Adv. 14 (2024) 9805–9818, https://doi.org/10.1039/d4ra00224e.

[30] S.F. Hoefler, G. Trimmel, T. Rath, Progress on lead-free metal halide perovskites for photovoltaic applications: a review, Monatsh. Chem. - Chem. Mon. 148 (2017) 795–826, https://doi.org/10.1007/s00706-017-1933-9.

[31] M. Roknuzzaman, K. Ostrikov, H. Wang, A. Du, T. Tesfamichael, Towards lead-free perovskite photovoltaics and optoelectronics by ab-initio simulations, Sci. Rep. 7 (2017) 14025, https://doi.org/10.1038/s41598-017-13172-y.

[32] S.J. Clark, M.D. Segall, C.J. Pickard, P.J. Hasnip, M.I.J. Probert, K. Refson, M.C. Payne, First principles methods using CASTEP, Z. für Kristallogr. - Cryst. Mater. 220 (2005) 567–570, https://doi.org/10.1524/zkri.220.5.567.65075.

[33] M.S. Daw, M.I. Baskes, Semiempirical, quantum mechanical calculation of hydrogen embrittlement in metals, Phys. Rev. Lett. 50 (1983) 1285–1288, https://doi.org/10.1103/PhysRevLett.50.1285.

[34] W. Kohn, Density functional and density matrix method scaling linearly with the number of atoms, Phys. Rev. Lett. 76 (1996) 3168–3171, https://doi.org/10.1103/PhysRevLett.76.3168.

[35] J.P. Perdew, K. Burke, M. Ernzerhof, Generalized gradient approximation made simple, Phys. Rev. Lett. 77 (1996) 3865–3868, https://doi.org/10.1103/PhysRevLett.77.3865.

[36] D. Vanderbilt, Soft self-consistent pseudopotentials in a generalized eigenvalue formalism, Phys. Rev. B 41 (1990) 7892–7895, https://doi.org/10.1103/PhysRevB.41.7892.

[37] T.H. Fischer, J. Almlof, General methods for geometry and wave function optimization, J. Phys. Chem. 96 (1992) 9768–9774, https://doi.org/10.1021/j100203a036.

[38] H.J. Monkhorst, J.D. Pack, Special points for Brillouin-zone integrations, Phys. Rev. B 13 (1976) 5188–5192, https://doi.org/10.1103/PhysRevB.13.5188.

[39] J. Kang, E.-C. Lee, K.J. Chang, First-principles study of the structural phase transformation of hafnia under pressure, Phys. Rev. B 68 (2003) 054106, https://doi.org/10.1103/PhysRevB.68.054106.

[40] F.D. Murnaghan, The compressibility of media under extreme pressures, Proc. Natl. Acad. Sci. USA 30 (1944) 244–247, https://doi.org/10.1073/pnas.30.9.244.

[41] MdS. Alam, M. Saiduzzaman, A. Biswas, T. Ahmed, A. Sultana, K.M. Hossain, Tuning band gap and enhancing optical functions of AGeF3 (A = K, Rb) under pressure for improved optoelectronic applications, Sci. Rep. 12 (2022) 8663, https://doi.org/10.1038/s41598-022-12713-4.

[42] M. Aktary, M. Kamruzzaman, R. Afrose, Pressure-dependent comparative study of the mechanical, electronic, and optical properties of CsPbX $_3$ (X = Cl, Br, I): a DFT study for optoelectronic applications, Mater. Adv. 4 (2023) 4494–4508, https://doi.org/10.1039/D3MA00311F.

[43] MdF. Rahman, MdH. Rahman, MdR. Islam, M.K. Hossain, A. Ghosh, MdS. Islam, MdM. Islam, Md Harun-Or-Rashid, H. Albalawi, Q. Mahmood, The optical and electronic properties of inorganic halide perovskite Sr3NCl3 under applied biaxial strain, J. Mater. Sci. 58 (2023) 13100–13117, https://doi.org/10.1007/s10853-023-08825-5.

[44] A.M. Humada, M. Hojabri, S. Mekhilef, H.M. Hamada, Solar cell parameters extraction based on single and double-diode models: a review, Renew. Sustain. Energy Rev. 56 (2016) 494–509, https://doi.org/10.1016/j.rser.2015.11.051.
[45] MdR. Islam, A.S.M.J. Islam, K. Liu, Z. Wang, S. Qu, C. Zhao, X. Wang, Z. Wang, Strain-induced tunability of the optoelectronic properties of inorganic lead iodide perovskites APbI3 (A= Rb and Cs), Phys. B Condens. Matter 638 (2022) 413960, https://doi.org/10.1016/j.physb.2022.413960.
[46] MdA.B. Shanto, MdF. Rahman, MdR. Islam, A. Ghosh, A. Azzouz-Rached, H. Albalawi, Q. Mahmood, Investigating how the electronic and optical properties of a novel cubic inorganic halide perovskite, Sr3NI3 are affected by strain, F1000Res. 12 (2023) 1005, https://doi.org/10.12688/f1000research.137044.1.
[47] Md Rasheduzzaman, K.M. Hossain, S.K. Mitro, M.A. Hadi, J.K. Modak, MdZ. Hasan, Structural, mechanical, thermal, and optical properties of inverse-Heusler alloys Cr2CoZ (Z = Al, In): a first-principles investigation, Phys. Lett. A 385 (2021) 126967, https://doi.org/10.1016/j.physleta.2020.126967.
[48] M.J. Mehl, Pressure dependence of the elastic moduli in aluminum-rich Al-Li compounds, Phys. Rev. B 47 (1993) 2493–2500, https://doi.org/10.1103/PhysRevB.47.2493.
[49] F. Mouhat, F.-X. Coudert, Necessary and sufficient elastic stability conditions in various crystal systems, Phys. Rev. B 90 (2014) 224104, https://doi.org/10.1103/PhysRevB.90.224104.
[50] D.H. Chung, W.R. Buessem, The voigt-Reuss-Hill (VRH) approximation and the elastic moduli of polycrystalline ZnO, TiO2 (Rutile), and α-Al2O3, J. Appl. Phys. 39 (1968) 2777–2782, https://doi.org/10.1063/1.1656672.
[51] R. Hill, The elastic behaviour of a crystalline aggregate, Proc. Phys. Soc. 65 (1952) 349–354, https://doi.org/10.1088/0370-1298/65/5/307.
[52] M. Al-Fahdi, A. Rodriguez, T. Ouyang, M. Hu, High-throughput computation of new carbon allotropes with diverse hybridization and ultrahigh hardness, Crystals 11 (2021) 783, https://doi.org/10.3390/cryst11070783.
[53] S.F. Pugh, XCII. Relations between the elastic moduli and the plastic properties of polycrystalline pure metals, London, Edinburgh Dublin Phil. Mag. J. Sci. 45 (1954) 823–843, https://doi.org/10.1080/14786440808520496.
[54] R.L. Fleischer, R.S. Gilmore, R.J. Zabala, Elastic moduli of polycrystalline, high-temperature binary intermetallic compounds, Acta Metall. 37 (1989) 2801–2803, https://doi.org/10.1016/0001-6160(89)90314-3.
[55] X. Gao, Y. Jiang, R. Zhou, J. Feng, Stability and elastic properties of Y–C binary compounds investigated by first principles calculations, J. Alloys Compd. 587 (2014) 819–826, https://doi.org/10.1016/j.jallcom.2013.11.005.
[56] C.M. Zener, S. Siegel, Elasticity and anelasticity of metals, J. Phys. Colloid Chem. 53 (1949) 1468, https://doi.org/10.1021/j150474a017.
[57] R.K. Sharme, MdR. Islam, MdA. Sarker, Md Solayman, Md Al Momin, MdR. Islam, First-principles study on electronic, mechanical, and optical properties of pressure-induced vanadium-based perovskite KVO3, Phys. B Condens. Matter 681 (2024) 415785, https://doi.org/10.1016/j.physb.2024.415785.
[58] S.I. Ranganathan, M. Ostoja-Starzewski, Universal elastic anisotropy index, Phys. Rev. Lett. 101 (2008) 055504, https://doi.org/10.1103/PhysRevLett.101.055504.